

# A Next-to-Leading-Order Study of Dihadron Production

J.F. Owens

*Physics Department, Florida State University, Tallahassee, FL 32306*

(Dated: December 24, 2018)

## Abstract

The production of pairs of hadrons in hadronic collisions is studied using a next-to-leading-order Monte Carlo program based on the phase space slicing technique. Up-to-date fragmentation functions based on fits to LEP data are employed, together with several versions of current parton distribution functions. Good agreement is found with data for the dihadron mass distribution. A comparison is also made with data for the dihadron angular distribution. The scale dependence of the predictions and the dependence on the choices made for the fragmentation and parton distribution functions are also presented. The good agreement between theory and experiment is contrasted to the case for single  $\pi^0$  production where significant deviations between theory and experiment have been observed.

## I. INTRODUCTION

The many successes of QCD at describing large momentum transfer processes have helped establish it as the theory of the strong interactions. Indeed, largely due to this success, research concerning QCD has moved from testing the theory to testing the approximations used to obtain predictions from the theory. Even though the overall description of large momentum transfer processes appears to be satisfactory, there are still some systematic discrepancies between the theory and experiment. These include, for example, problems observed in direct photon production [1] and single  $\pi^0$  production [2]. One phenomenological approach has emphasized that the single particle production processes are sensitive to recoil corrections due to the emission of initial state radiation – also known as  $k_T$  smearing [3]. Another viewpoint [2] has stressed that, at least in the case of  $\pi^0$  production, there may be problems with our knowledge of the fragmentation functions in the region where the momentum fraction,  $z$ , taken by the produced particle is large, since this is a region where the data to which these functions are fitted are limited. Also, it has been noted that this same high- $z$  region may require significant threshold resummation corrections.

The production of hadron pairs relies on the same underlying dynamics as single particle production. Furthermore, the production of high-mass pairs relies on the same high- $z$  region of the fragmentation functions as does single particle production. Thus, if threshold corrections are important, or if the fragmentation functions are inadequately known, then one might expect to see comparable disagreement between the data for dihadron production and the predictions as one sees for single particle production.

It is the purpose of this paper to present a comparison between data for high-mass dihadron production and predictions based on QCD. These predictions have been obtained using a next-to-leading-order Monte Carlo based program which uses a variant of the phase space slicing technique [4, 5]. This allows the same kinematic cuts used in the extraction of the data to be imposed on the theoretical predictions.

The outline of the paper is as follows. In the next section a brief overview of the structure of the calculation is presented. Then, the predictions of the program are compared to data in Sec. III. A summary and some conclusions are presented in Sec. IV.

## II. NEXT-TO-LEADING-ORDER MONTE CARLO CALCULATION

The calculation described in this section is based on the two-cutoff phase space slicing technique described in [4, 5]. The basic concept is to partition the three-body phase space into three regions using two cutoff parameters,  $\delta_s$  and  $\delta_c$ . One region is where the  $2 \rightarrow 3$  matrix elements have soft or collinear singularities, one contains hard-collinear singularities, and in the remainder the matrix elements are finite. In the soft and hard-collinear regions the matrix elements are approximated using the soft or leading pole approximations, respectively, and the variables describing the soft or collinear quanta can be integrated over analytically. The results have the same form as the lowest order  $2 \rightarrow 2$  contributions, but depend explicitly on the cutoffs used to define the soft and hard-collinear regions. Likewise, the remaining finite  $2 \rightarrow 3$  contributions depend on the cutoffs used to isolate the divergent regions. These two types of contributions are used to generate two-body and three-body weights which are added together at the histogramming stage. For infrared-safe observables the dependence on the cutoffs cancels, provided that sufficiently small values of the cutoffs are chosen. Specific examples of this procedure are given in [5].

The case of high-mass dihadron production is formally rather similar to that for single hadron production with the addition of another fragmentation function. The treatment presented here, therefore, follows closely the presentation given in Sec. III E. of Ref. [5].

The input needed for this calculation includes the squared matrix elements for the  $2 \rightarrow 3$  subprocesses and the results for the  $\mathcal{O}(\alpha_s^3)$  one-loop contributions to the  $2 \rightarrow 2$  subprocesses [6, 7]. For the purpose of this example, the notation of [7] will be used, since much of the input needed can be found in the appendices of that paper. The partons are labelled as  $A + B \rightarrow 1 + 2$  and  $A + B \rightarrow 1 + 2 + 3$  for the  $2 \rightarrow 2$  and  $2 \rightarrow 3$  subprocesses, respectively. A flavor label  $a_A$  is used to denote the flavor of parton  $A$ , and similarly for the other partons.

The lowest-order contribution to the inclusive cross section for producing two hadrons  $h_1$  and  $h_2$  in a collision of hadrons of types  $A$  and  $B$  can be written as

$$d\sigma^B = \frac{1}{2x_A x_B s} \sum_{a_A, a_B, a_1, a_2} G_{a_A/A}(x_A) G_{a_B/B}(x_B) D_{h_1/a_1}(z_1) D_{h_2/a_2}(z_2) dx_A dx_B dz_1 dz_2 \times \frac{(4\pi\alpha_s)^2}{w(a_A)w(a_B)} \psi^{(4)}(\vec{a}, \vec{p}) d\Gamma_2 \quad (2.1)$$

where  $\vec{a} = \{a_A, a_B, a_1, a_2\}$  and  $\vec{p} = \{p_A^\mu, p_B^\mu, p_1^\mu, p_2^\mu\}$  denote the sets of flavor indices and parton four-vectors, respectively. The factors appearing in the spin/color averaging are

given by

$$w(a) = \begin{cases} 2(1 - \epsilon)V & \text{a=gluon} \\ 2N & \text{a=quark or antiquark} \end{cases}$$

with  $N = 3$  and  $V = N^2 - 1$ . The factor  $d\Gamma_2$  is the differential two-body phase space element in  $n$ -dimensions,

$$d\Gamma_2 = \frac{d^{n-1}p_3}{2p_3^0(2\pi)^{n-1}} \frac{d^{n-1}p_4}{2p_4^0(2\pi)^{n-1}} (2\pi)^n \delta^n(p_1 + p_2 - p_3 - p_4). \quad (2.2)$$

Eq. (2.1) gives the contribution where parton 1 fragments into the hadron  $h_1$  and parton 2 fragments into  $h_2$ . Care must be taken to explicitly include in the sum over  $\vec{a}$  those terms corresponding to the case where parton 2 fragments into  $h_1$  and vice versa. For compactness, these terms will not be explicitly written. The squared matrix elements for the various subprocesses, denoted by  $\psi^{(4)}(\vec{a}, \vec{p})$ , may be found in Ref. [7].

Next, consider the one-loop virtual corrections to the  $2 \rightarrow 2$  subprocesses. These take the form

$$d\sigma^v = \frac{1}{2x_A x_B s} \sum_{a_A, a_B, a_1, a_2} G_{a_A/A}(x_A) G_{a_B/B}(x_B) D_{h_1/a_1}(z_1) D_{h_2/a_2}(z_2) dx_A dx_B dz_1 dz_2 \\ \times \frac{(4\pi\alpha_s)^2}{w(a_A)w(a_B)} \left[ \frac{\alpha_s}{2\pi} \left( \frac{4\pi\mu_R^2}{2p_A \cdot p_B} \right)^\epsilon \frac{\Gamma(1-\epsilon)}{\Gamma(1-2\epsilon)} \right] \psi^{(6)}(\vec{a}, \vec{p}) d\Gamma_2 \quad (2.3)$$

where

$$\psi^{(6)}(\vec{a}, \vec{p}) = \psi^{(4)}(\vec{a}, \vec{p}) \left[ -\frac{1}{\epsilon^2} \sum_n C(a_n) - \frac{1}{\epsilon} \sum_n \gamma(a_n) \right] \\ + \frac{1}{2\epsilon} \sum_{\substack{m,n \\ m \neq n}} \ln \left( \frac{p_m \cdot p_n}{p_A \cdot p_B} \right) \psi_{m,n}^{(4,c)}(\vec{a}, \vec{p}) \\ - \frac{\pi^2}{6} \sum_n \psi^{(4)}(\vec{a}, \vec{p}) + \psi_{NS}^{(6)}(\vec{a}, \vec{p}) + \mathcal{O}(\epsilon). \quad (2.4)$$

This expression for  $\psi^{(6)}$  differs slightly from Eq. (35) in Ref. [7] because we have chosen to extract a different  $\epsilon$  dependent overall factor: a factor of  $\Gamma(1+\epsilon)\Gamma(1-\epsilon) \approx 1 + \epsilon^2 \frac{\pi^2}{6}$  has been absorbed into the above expression for  $\psi^{(6)}$ . Furthermore, the arbitrary scale  $Q_{ES}^2$  used in Ref. [7] has been chosen to be  $2p_A \cdot p_B$ . The expressions for the functions  $\psi_{m,n}^{(4,c)}$  and  $\psi_{NS}^{(6)}$  may be found in Appendix B of Ref. [7]. The quantities  $C(a_n)$  and  $\gamma(a_n)$  are given by

$$C(a) = \begin{cases} N = 3 & \text{a=gluon} \\ C_F = \frac{4}{3} & \text{a=quark or antiquark} \end{cases}$$

and

$$\gamma(a) = \begin{cases} (11N - 2n_f)/6 & \text{a=gluon} \\ 3C_F/2 & \text{a=quark or antiquark} \end{cases}$$

It will be convenient for subsequent expressions to adopt the following notation:

$$\mathcal{F} = \left( \frac{4\pi\mu_R^2}{2p_A \cdot p_B} \right)^\epsilon \frac{\Gamma(1-\epsilon)}{\Gamma(1-2\epsilon)}. \quad (2.5)$$

The one loop virtual contributions can now be written as

$$\begin{aligned} d\sigma^v &= \frac{1}{2x_A x_B s} \sum_{a_A, a_B, a_1, a_2} G_{a_A/A}(x_A) G_{a_B/B}(x_B) D_{h_1/a_1}(z_1) D_{h_2/a_2}(z_2) dx_A dx_B dz_1 dz_2 \\ &\times \frac{(4\pi\alpha_s)^2}{w(a_A)w(a_B)} \mathcal{F} \frac{\alpha_s}{2\pi} \left( \frac{A_2^v}{\epsilon^2} + \frac{A_1^v}{\epsilon} + A_0^v \right) d\Gamma_2 \end{aligned} \quad (2.6)$$

where

$$A_2^v = - \sum_n C(a_n) \psi^{(4)}(\vec{a}, \vec{p}) \quad (2.7)$$

$$A_1^v = - \sum_n \gamma(a_n) \psi^{(4)}(\vec{a}, \vec{p}) + \frac{1}{2} \sum_{\substack{m,n \\ m \neq n}} \ln \left( \frac{p_m \cdot p_n}{p_A \cdot p_B} \right) \psi_{m,n}^{(4,c)}(\vec{a}, \vec{p}) \quad (2.8)$$

$$A_0^v = - \frac{\pi^2}{6} \sum_n C(a_n) \psi^{(4)}(\vec{a}, \vec{p}) + \psi_{NS}^{(6)}(\vec{a}, \vec{p}). \quad (2.9)$$

Next, the contributions from the  $2 \rightarrow 3$  subprocesses in the limit where one of the final state gluons becomes soft are needed. The contributions of the  $2 \rightarrow 3$  subprocesses may be written as

$$\begin{aligned} d\sigma^{2 \rightarrow 3} &= \frac{1}{2x_A x_B s} \frac{(4\pi\alpha_s)^3}{w(a_A)w(a_B)} \mathcal{F} \sum_{a_A, a_B, a_1, a_2, a_3} G_{a_A/A}(x_A) G_{a_B/B}(x_B) D_{h_1/a_1}(z_1) D_{h_2/a_2}(z_2) \\ &\times \Psi(a_A, a_B, a_1, a_2, a_3, p_A^\mu, p_B^\mu, p_1^\mu, p_2^\mu, p_3^\mu) d\Gamma_3 dx_A dx_B dz_1 dz_2. \end{aligned} \quad (2.10)$$

The expressions for the  $2 \rightarrow 3$  squared matrix elements appearing in Eq. (2.10) may be found in Ref. [6]. As noted earlier for the two-body contributions, one must include in the sum all possible parton to hadron fragmentations. Here  $d\Gamma_3$  is the three-body invariant phase space factor in  $n$ -dimensions:

$$d\Gamma_3 = \frac{d^{n-1}p_3}{2p_3^0(2\pi)^{n-1}} \frac{d^{n-1}p_4}{2p_4^0(2\pi)^{n-1}} \frac{d^{n-1}p_5}{2p_5^0(2\pi)^{n-1}} (2\pi)^n \delta^n(p_1 + p_2 - p_3 - p_4 - p_5). \quad (2.11)$$

Consider the case where the soft gluon is parton 3. In this limit, the function  $\Psi$  may be expanded as:

$$\Psi(a_A, a_B, a_1, a_2, a_3, p_A^\mu, p_B^\mu, p_1^\mu, p_2^\mu, p_3^\mu) \sim \sum_{\substack{m,n \\ m < n}} \delta_{a_3,g} \frac{p_m \cdot p_n}{p_m \cdot p_3 p_n \cdot p_3} \psi_{m,n}^{(4,c)}(a_A, a_B, a_1, a_2, p_A^\mu, p_B^\mu, p_1^\mu, p_2^\mu). \quad (2.12)$$

Next, one must integrate over the soft region of phase space defined by  $E_3 < \delta_s \sqrt{2p_A \cdot p_B}/2$ . This is easily done using the integrals given in the appendix of Ref. [5]. The resulting soft contribution may be written as

$$d\sigma^s = \frac{1}{2x_A x_B s} \sum_{a_A, a_B, a_1, a_2} G_{a_A/A}(x_A) G_{a_B/B}(x_B) D_{h_1/a_1}(z_1) D_{h_2/a_2}(z_2) dx_A dx_B dz_1 dz_2 \\ \times \frac{(4\pi\alpha_s)^2}{w(a_A)w(a_B)} \mathcal{F} \frac{\alpha_s}{2\pi} \left( \frac{A_2^s}{\epsilon^2} + \frac{A_1^s}{\epsilon} + A_0^s \right) d\Gamma_2 \quad (2.13)$$

where

$$A_2^s = \sum_n C(a_n) \psi^{(4)}(\vec{a}, \vec{p}) \quad (2.14)$$

$$A_1^s = -2 \ln \delta_s \sum_n C(a_n) \psi^{(4)}(\vec{a}, \vec{p}) - \frac{1}{2} \sum_{\substack{m,n \\ m \neq n}} \ln \left( \frac{p_m \cdot p_n}{p_A \cdot p_B} \right) \psi_{m,n}^{(4,c)}(\vec{a}, \vec{p}) \quad (2.15)$$

$$A_0^s = 2 \ln^2 \delta_s \sum_n C(a_n) \psi^{(4)}(\vec{a}, \vec{p}) \\ + \left( \psi_{A,1}^{(4,c)} + \psi_{B,2}^{(4,c)} \right) \left[ \frac{1}{2} \ln^2 \left( \frac{p_1 \cdot p_3}{p_A \cdot p_B} \right) + \text{Li}_2 \left( \frac{p_2 \cdot p_3}{p_A \cdot p_B} \right) + 2 \ln \delta_s \ln \left( \frac{p_1 \cdot p_3}{p_A \cdot p_B} \right) \right] \\ + \left( \psi_{A,2}^{(4,c)} + \psi_{B,1}^{(4,c)} \right) \left[ \frac{1}{2} \ln^2 \left( \frac{p_2 \cdot p_3}{p_A \cdot p_B} \right) + \text{Li}_2 \left( \frac{p_1 \cdot p_3}{p_A \cdot p_B} \right) + 2 \ln \delta_s \ln \left( \frac{p_2 \cdot p_3}{p_A \cdot p_B} \right) \right]. \quad (2.16)$$

After the collinear singularities associated with the parton distribution functions and fragmentation function have been factorized and absorbed into the corresponding bare functions, there will be soft-collinear terms left over due to the mismatch between the integration limits of the collinear singularity terms and the factorization counterterms. Collecting together the various collinear terms, the result can be written as follows:

$$d\sigma^{coll} = \frac{1}{2x_A x_B s} \sum_{a_A, a_B, a_1, a_2} G_{a_A/A}(x_A) G_{a_B/B}(x_B) D_{h_1/a_1}(z_1) D_{h_2/a_2}(z_2) dx_A dx_B dz_1 dz_2 \\ \times \frac{(4\pi\alpha_s)^2}{w(a_A)w(a_B)} \mathcal{F} \frac{\alpha_s}{2\pi} \left( \frac{A_1^{coll}}{\epsilon} + A_0^{coll} \right) d\Gamma_2 \quad (2.17)$$

where

$$A_1^{coll} = \sum_n [2 \ln \delta_s C(a_n) + \gamma(a_n)] \quad (2.18)$$

$$A_0^{coll} = \sum_{n=A,B} [2 \ln \delta_s C(a_n) + \gamma(a_n)] \ln \left( \frac{2p_A \cdot p_B}{\mu_f^2} \right) \\ + \sum_{n=1,2} [2 \ln \delta_s C(a_n) + \gamma(a_n)] \ln \left( \frac{2p_A \cdot p_B}{M_f^2} \right). \quad (2.19)$$

Here  $\mu_f$  and  $M_f$  are the initial and final state factorization scales.

After the mass factorization has been performed, the bare parton distribution functions and fragmentation functions have been replaced by scale dependent  $\overline{\text{MS}}$  functions. In addition, there are finite remainders involving functions  $\tilde{G}$  and  $\tilde{D}$ , expressions for which may be found in [5]:

$$\begin{aligned}
d\tilde{\sigma} = & \frac{1}{2x_A x_B s} \sum_{a_A, a_B, a_1, a_2} \frac{(4\pi\alpha_s)^2}{w(a_A)w(a_B)} \frac{\alpha_s}{2\pi} \psi^{(4)}(\vec{a}, \vec{p}) dx_A dx_B dz_1 dz_2 d\Gamma_2 \\
& \times \left[ \tilde{G}_{a_A/A}(x_A, \mu_f^2) G_{a_B/B}(x_B, \mu_f^2) D_{h_1/a_1}(z_1, M_f^2) D_{h_2/a_2}(z_2, M_f^2) \right. \\
& + G_{a_A/A}(x_A, \mu_f^2) \tilde{G}_{a_B/B}(x_B, \mu_f^2) D_{h_1/a_1}(z_1, M_f^2) D_{h_2/a_2}(z_2, M_f^2) \\
& + G_{a_A/A}(x_A, \mu_f^2) G_{a_B/B}(x_B, \mu_f^2) \tilde{D}_{h_1/a_1}(z_1, M_f^2) D_{h_2/a_2}(z_2, M_f^2) \\
& \left. + G_{a_A/A}(x_A, \mu_f^2) G_{a_B/B}(x_B, \mu_f^2) D_{h_1/a_1}(z_1, M_f^2) \tilde{D}_{h_2/a_2}(z_2, M_f^2) \right]. \quad (2.20)
\end{aligned}$$

At this point, all of the singular terms have been isolated as poles in  $\epsilon$  or have been factorized and absorbed into the bare parton distribution and fragmentation functions. The  $\epsilon$  dependent pole terms all cancel amongst each other:

$$A_2^v + A_2^s = 0 \quad (2.21)$$

$$A_1^v + A_1^s + A_1^{coll} = 0. \quad (2.22)$$

The finite two-body contribution is given by

$$\begin{aligned}
d\sigma^{2 \rightarrow 2} = & d\sigma^B + d\tilde{\sigma} \\
& + \frac{1}{x_A x_B s} \sum_{a_A, a_B, a_1, a_2} \frac{(4\pi\alpha_s)^2}{w(a_A)w(a_B)} G_{a_A/A}(x_A, \mu_f^2) G_{a_B/B}(x_B, \mu_f^2) \\
& \times D_{h_1/a_1}(z_1, M_f^2) D_{h_2/a_2}(z_2, M_f^2) \frac{\alpha_s}{2\pi} \left[ A_0^v + A_0^s + A_0^{coll} \right] dx_A dx_B dz_1 dz_2 d\Gamma_2. \quad (2.23)
\end{aligned}$$

The three-body contribution, now evaluated in four dimensions, was given in Eq. (2.10) where now the soft and collinear regions of phase space are excluded.

The structure of the final result is two finite contributions, both of which depend on the soft and collinear cutoffs – one explicitly and one through the boundaries imposed on the three-body phase space. However, when both contributions are added while calculating an observable quantity, all dependence on the cutoffs cancels when sufficiently small values of the cutoffs are used.

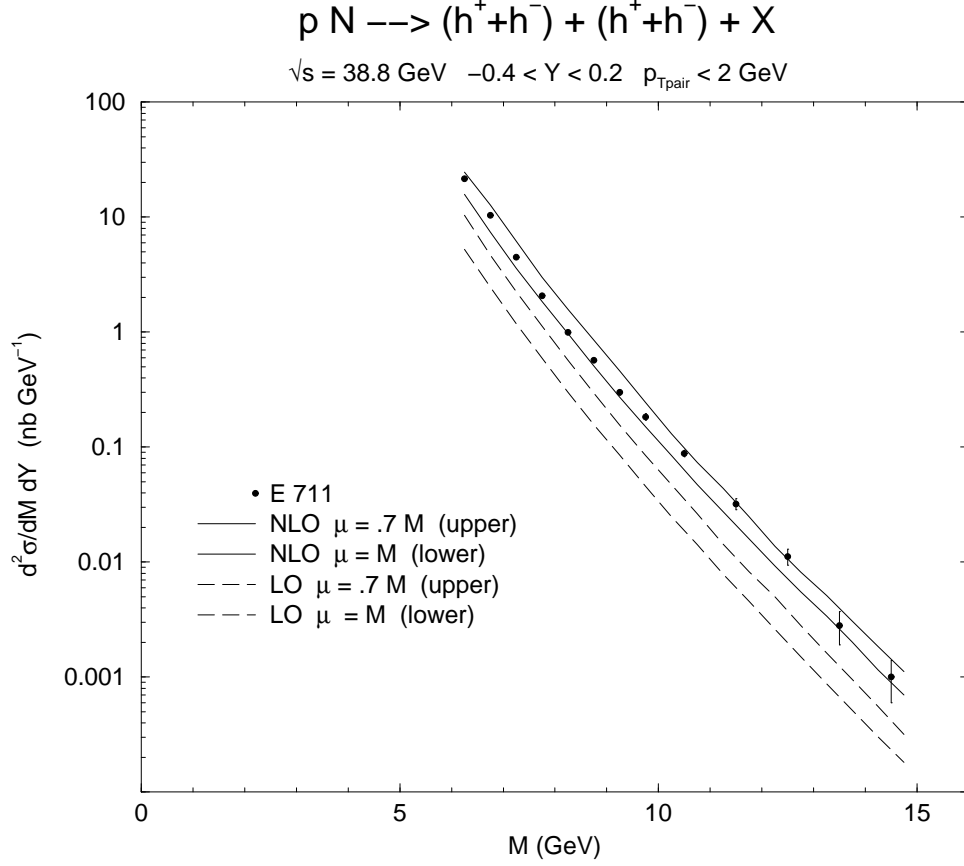


FIG. 1: Comparison of the NLO(solid) and LO(dashed) results with data from the E-711 experiment [13].

### III. COMPARISON TO DATA

Two sets of next-to-leading-order fragmentation functions have become available recently [8, 9]. Both sets have been fit to high statistics data from  $e^+e^-$  experiments. Accordingly, only charge symmetric combinations, e.g.,  $h^+ + h^-$ , have been determined and the sets do not have fragmentation functions for individual charge states. Nevertheless, these sets can be used to generate predictions for experiments which measured either  $\pi^0\pi^0$  final states or symmetric combinations of charged hadrons. The NA-24 [10], CCOR [11], and E-706 [12] experiments each measured the production of  $\pi^0$  pairs while the E-711 [13] experiment measured the production of  $h^+h^+$ ,  $h^-h^-$ , and  $h^+h^-$  pairs. In the latter case, one can combine the tabulated results to give the cross section for producing the symmetric combination  $(h^+ + h^-) + (h^+ + h^-)$ .

In the following, unless otherwise stated, the theoretical results have been obtained using



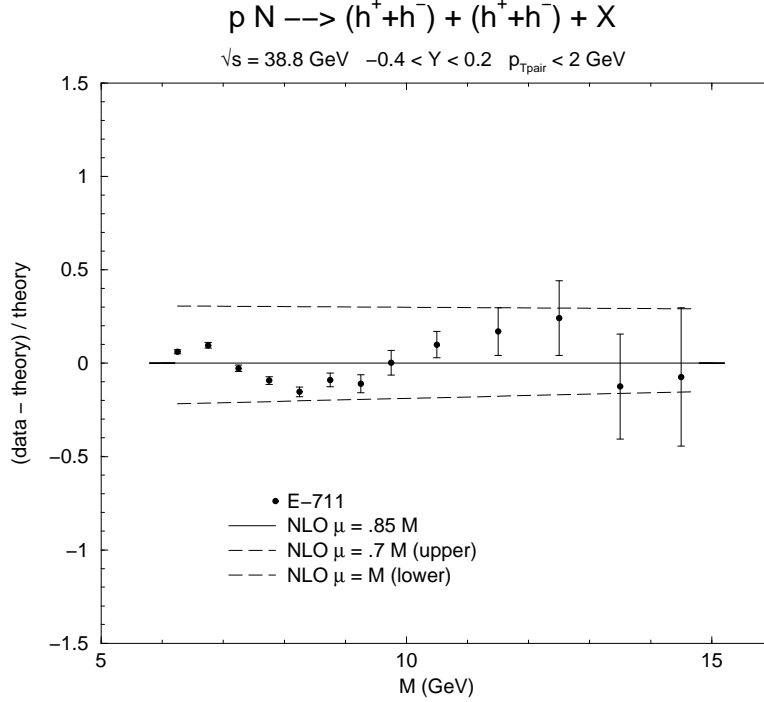


FIG. 2: CTEQ5M results compared to the E-711 data for different scale choices. The renormalization and initial and final state factorization scales have been set equal to each other.

the CTEQ5M [14] parton distributions and the KKP [8] fragmentation functions. For the calculation of the cross section at fixed values of the dihadron mass,  $M$ , the renormalization and factorization scales have been chosen to be proportional to  $M$ , as this is the only observed hadronic variable with the appropriate dimension.

In FIG. 1 the E-711 [13] data are shown with the leading-order (LO) and next-to-leading-order (NLO) theoretical results with two choices for the common factorization and renormalization scales. Cuts were applied to the rapidity of the pair,  $Y$ , the transverse momentum of the pair,  $p_{Tpair}$ , and  $\cos \theta^*$ , an estimate of the cosine of the scattering angle in the parton-parton center of mass frame. For these data,  $\cos \theta^*$  was defined by first transforming to the frame where the momentum of the hadron pair had no longitudinal component. In general, the two hadrons will not be exactly back-to-back in this frame, due to their differing values of transverse momentum. The two values of the cosine of the angle between the hadron direction and the beam direction were averaged to obtain  $\cos \theta^*$ . The cuts used for the data shown in FIG. 1 were  $-0.4 < Y < 0.2$ ,  $p_{Tpair} < 2$  GeV and  $|\cos \theta^*| < 0.25$ . The NLO results can be seen to bracket the data while, for the scale choices shown, the LO results are significantly below the data. The large scale dependence evident at lowest order is due

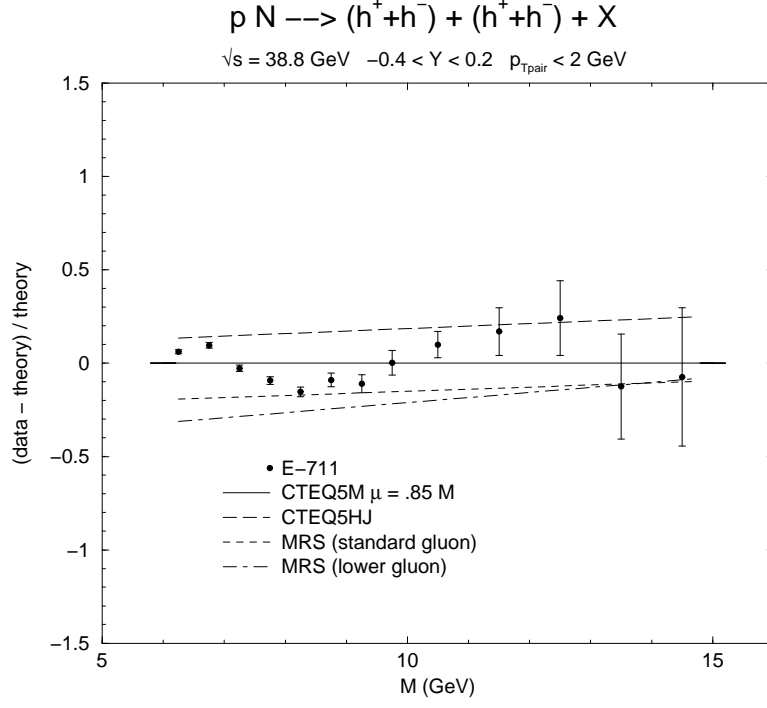


FIG. 3: Comparison between the CTEQ5M predictions with those from the CTEQ5HJ [14] set and several MRST [15] sets.

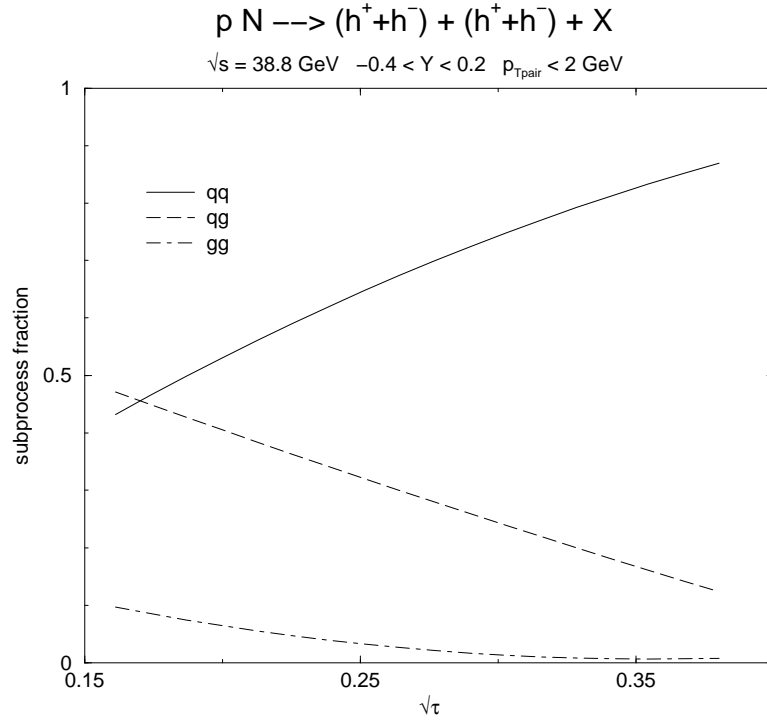


FIG. 4: Relative contributions of the  $qq$ ,  $qg$ , and  $gg$  subprocesses to the CTEQ5M results with  $\mu = 0.85M$ .

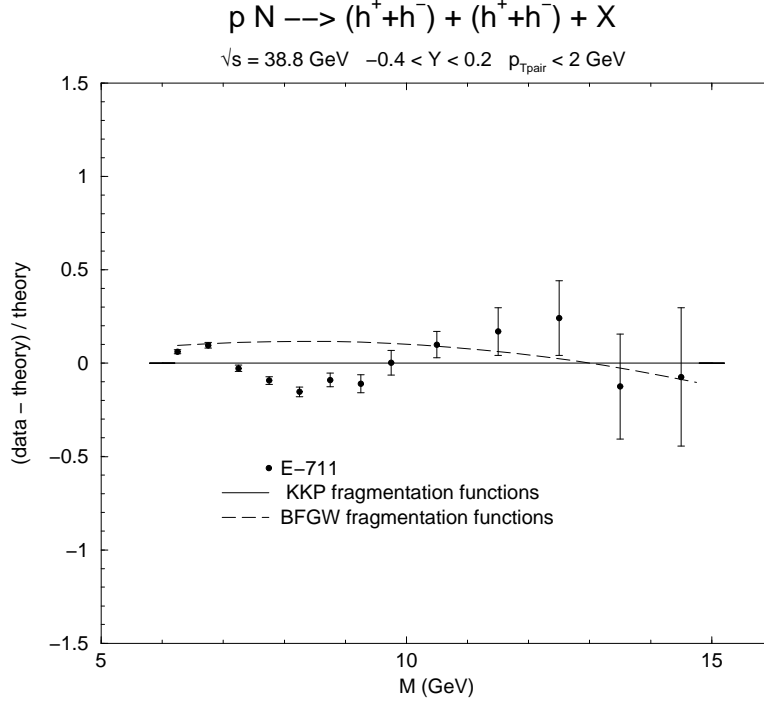


FIG. 5: Comparison between the results obtained using the KKP [8] and BFGW [9] fragmentation functions.

to the two powers of  $\alpha_s$  in combination with the scale dependence of the four distribution and fragmentation functions. In the kinematic regime covered by the data, the distribution and fragmentation function momentum fractions are large, so that the functions decrease with increasing values of the scale. These scale dependences result in a significant decrease of the cross section with increasing scale, as shown in FIG. 1. The band covered by the corresponding NLO curves is narrower, although significant scale dependence remains. This is further examined in FIG. 2 where the NLO results are compared to the E-711 data for three choices of scale. The format  $(\text{data-theory})/\text{theory}$  is used in order to more clearly show the scale dependence.

In FIG. 3 the dependence of the results on variations in the choice of parton distributions is shown, relative to the CTEQ5M results. For each curve the scale has been set to  $\mu = 0.85M$ . The CTEQ5HJ set [14] has a gluon distribution which has been enhanced in the high- $x$  region in order to better describe the high- $E_T$  jet data from the CDF and DØ Collaborations. Relative to the CTEQ5M distribution results, one can see an overall increase in the cross section, with the increase becoming larger towards the high mass end. Note that an increase in the scale from  $0.85M$  to  $M$  would bring the CTEQ5HJ curve down to the level of the

data. Also shown are the results for two of the MRST [15] sets, one with the standard gluon and one with a reduced gluon. Although the two curves lie below the CTEQ5M results, a modest decrease in the scale choice would raise the curves to be in accord with the data. The results for a third MRST set with an increased gluon distribution are essentially identical with the CTEQ5M results.

In FIG. 4 the relative contributions of the quark-quark, quark-gluon, and gluon-gluon subprocesses are shown versus  $\sqrt{\tau} = M/\sqrt{s}$ . This dimensionless variable is approximately the value of the parton momentum fraction which is probed in the production of the high mass hadron pair. As expected, quark-quark scattering dominates at the upper end of the mass range covered by the data. Nevertheless, there is a significant contribution from quark-gluon scattering over much of the mass range. This is similar to the situation for high- $E_T$  jet production and, indeed, the results in FIG. 3 do show some sensitivity to the choice of the parton distributions, e.g., CTEQ5M *vs.* CTEQ5HJ. Unfortunately, the scale dependence, even at NLO, is such as to preclude favoring one set over the other.

Next, in FIG. 5 the dependence on the choice of the fragmentation functions is shown. The results from the two sets agree to within about 10% across the mass range shown.

From the results shown thus far, several conclusions can be drawn. First, the NLO results give a very good description of the mass distribution for symmetric hadron pairs measured by the E-711 Collaboration. The variations observed due to different choices of the distribution and fragmentation functions are easily compensated for by changes in the renormalization and factorization scales. Nevertheless, extreme variations of these scales are not needed in order to describe the data.

Next, consider the data for producing pairs of neutral pions. In FIG. 6 the theoretical results are compared to data for the process  $pp \rightarrow \pi^0\pi^0 + X$  as measured by the NA-24 [10] and CCOR [11] Collaborations. The cuts used for these data are  $-0.35 < Y < 0.35$ ,  $p_{T_{pair}} < 1$ , and  $|\cos\theta^*| < 0.4$ . The same scale choice of  $\mu = 0.85M$  as used for the E-711 data gives a good description of the experimental results. Again, the CTEQ5M and KKP distribution and fragmentation functions have been used. The same results are shown in FIG. 7 in a data/theory format versus  $\sqrt{\tau}$ . For the NA-24 data, the statistical and systematic errors have been added in quadrature. No discussion of errors was contained in the CCOR paper [11]. However, in an earlier publication on single  $\pi^0$  production the CCOR Collaboration quotes an overall error of 25% for both energies with an additional 5% relative normalization

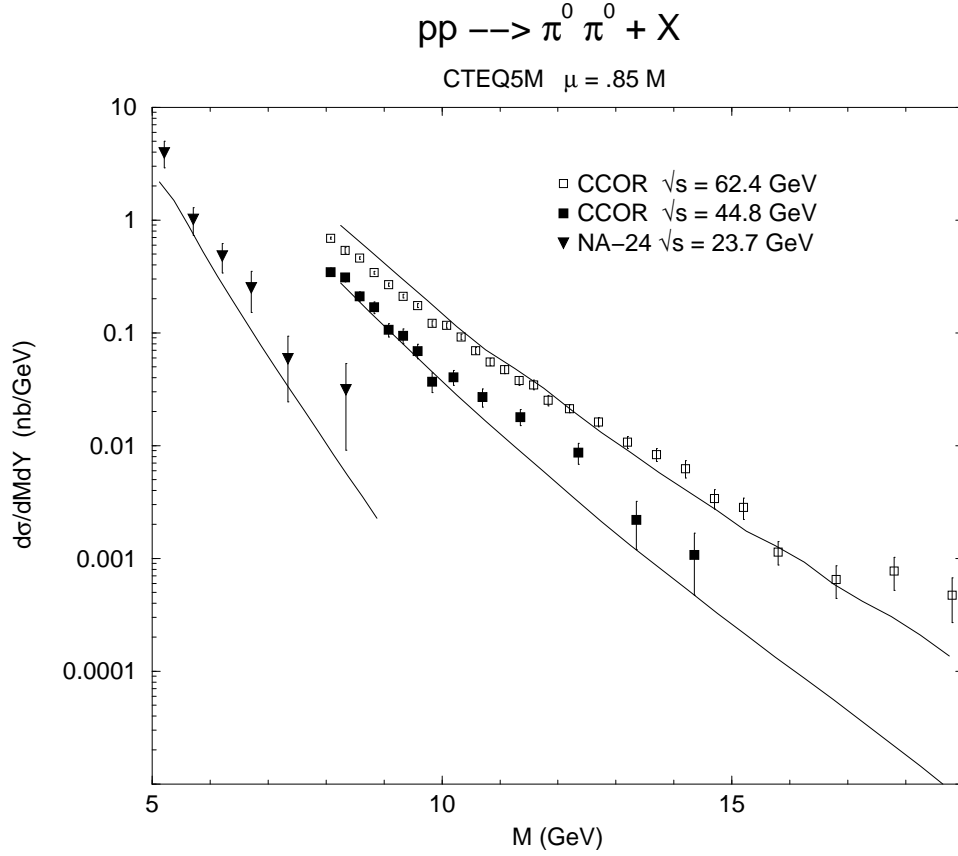


FIG. 6: Comparison between the CTEQ5M results and data from the NA-24 [10] and CCOR [11] Collaborations.

error between the results for the two energies. Thus, the three data sets are seen to agree within the quoted errors. Furthermore, given these errors, the agreement with the theoretical results is acceptable, although deviations are apparent in FIGS. 6 and 7.

Noting the tendency for the data to lie below the theory for small  $\sqrt{\tau}$  and above it for larger  $\sqrt{\tau}$ , it is natural to ask whether the CTEQ5HJ distributions might yield better agreement with the data. These results are shown in FIG. 8 with a scale choice of  $\mu = M$ . Although the agreement is slightly better, the modified gluon distribution is unable to bring the theory and the data into complete agreement. Nevertheless, given the size of the errors, no definitive conclusion can be drawn.

In FIG. 9 the NLO predictions are compared with data for dipion production as measured by the E-706 Collaboration [12]. For these data the pions were separately required to satisfy  $p_T > 2.5$  GeV and  $-0.8 < y < 0.8$  ( $-1.05 < y < 0.55$ ) for the  $\sqrt{s} = 31.6$  (38.8) GeV data. The difference between the azimuthal angles for the two pions,  $\Delta\phi$ , was required to

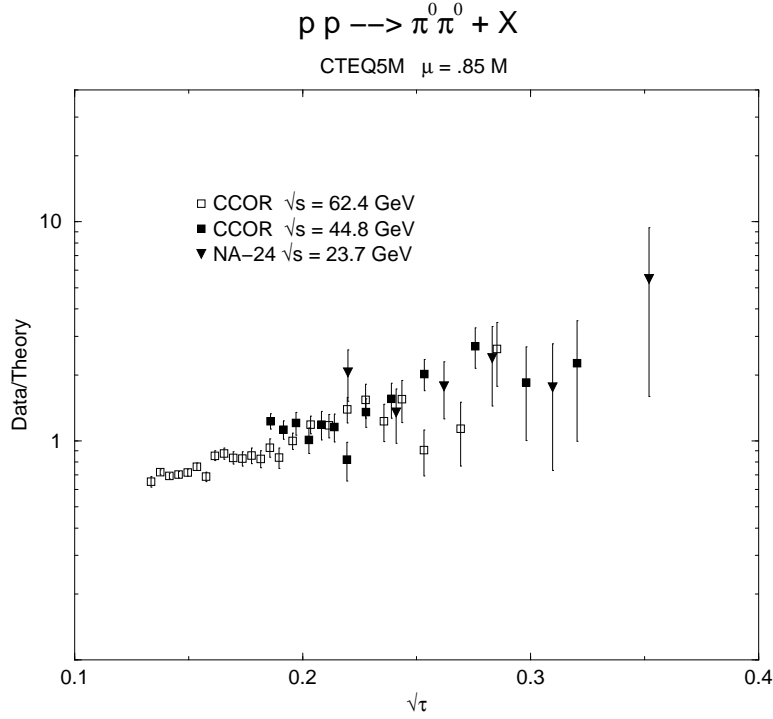


FIG. 7: The same as for FIG. 6 presented in the data/theory format.

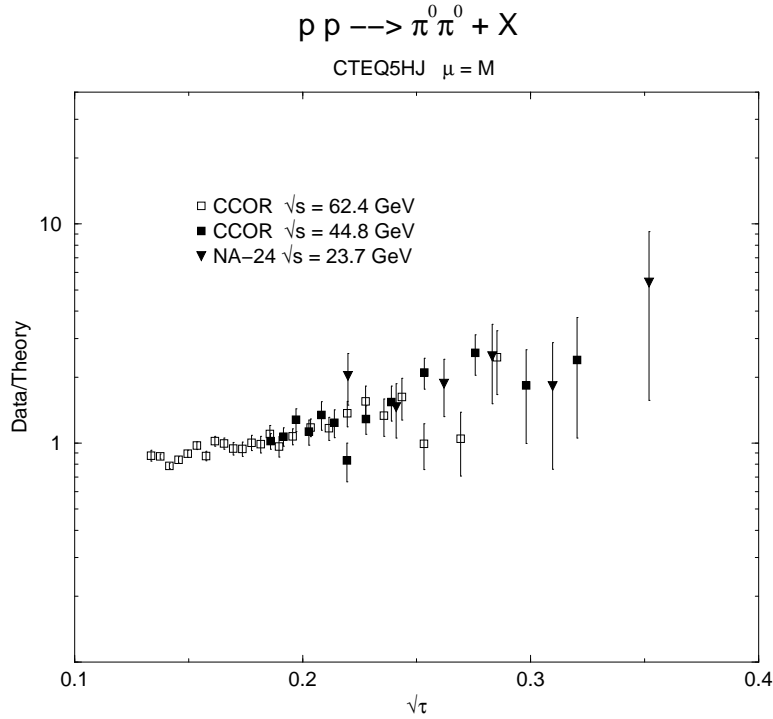


FIG. 8: The same as for FIG. 7 except using the CTEQ5HJ distributions.

be greater than 105 degrees. No cuts were placed on  $\cos \theta^*$  or on  $p_{Tpair}$ . There is good agreement between the theory and the data when a scale choice of  $\mu = 0.35M$  is used. This

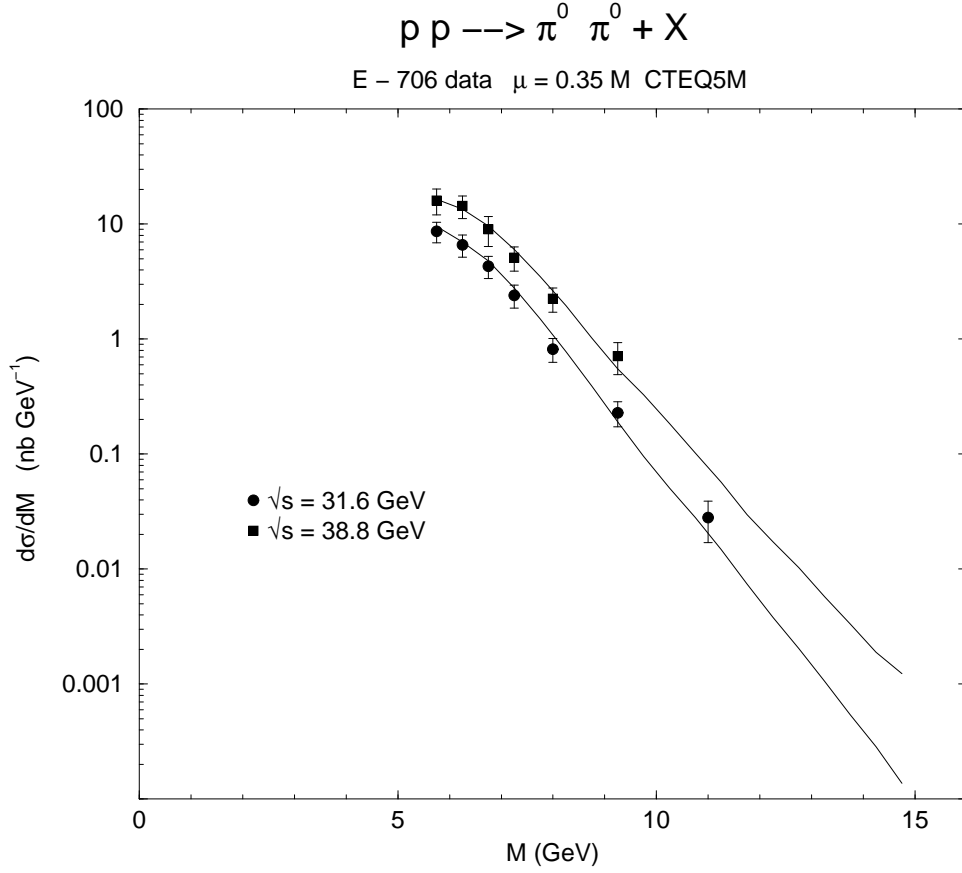


FIG. 9: Comparison between the NLO results and data from the E-706 Collaboration [12].

value is significantly smaller than that used in the previous comparisons. Of course, the cuts used for the E-706 data set are far different than those used for the other sets. As a consistency check on their data the E-706 Collaboration [12] also presented results obtained using cuts similar to those used for the E-711 data. These data are compared to the NLO predictions in FIG. 10 with  $\mu = 0.50 M$  and  $0.85 M$ . The two curves bracket the data, suggesting that E706 results are compatible with those of the other experiments when the same cuts are used. This suggests that the need for a much smaller scale when comparing with the E-706 data in FIG. 9 is a problem due to the calculation not being able to properly reproduce the effects of the different sets of cuts.

In order to investigate this situation further, consider the effects of a cut in  $\Delta\phi$ . The significance of the  $\Delta\phi$  cuts lies in the fact that the observed  $\Delta\phi$  distributions are broader than those given by the NLO calculations, as can be seen in FIGS. 11 and 12. At lowest order, with collinear fragmentation and distribution functions, the theoretical predictions have the two hadrons being produced back-to-back, *i.e.*, with  $\Delta\phi = 180$  degrees. At next-

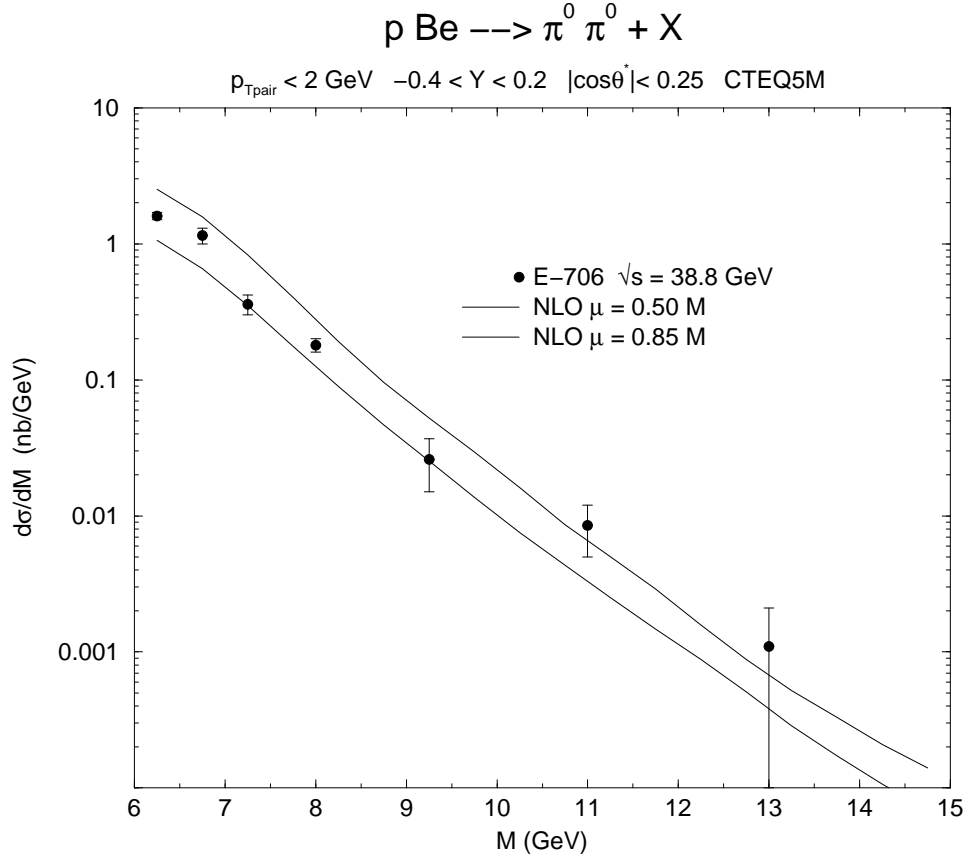


FIG. 10: Comparison between the NLO results and data from the E-706 Collaboration [12].

to-leading-order, the  $2 \rightarrow 3$  subprocesses allow for the  $\Delta\phi$  distribution to develop a non-zero width. Nevertheless, it is still narrower than the experimental observations. The acceptance for the CCOR and E-711 experiments was limited to  $\Delta\phi > 140$  degrees, and this cut was also placed on the NA-24 data shown previously, so essentially none of the NLO generated cross section was rejected. Opening up the cuts to the value  $\Delta\phi > 105$  degrees used by the E-706 experiment does not, therefore, result in any increase of the theoretical cross section. However, it does result in an increase in the experimental cross section. The net result is that the NLO calculation will not correctly reproduce the effects of different  $\Delta\phi$  cuts because the theoretical distribution is too narrow. This results in a relative normalization shift when comparing experiments which used different cuts in  $\Delta\phi$ . This shift can be accommodated by altering the renormalization and factorization scales used in the theoretical calculations. Alternatively, one can restrict the comparison to data sets which use the same  $\Delta\phi$  cut. Similar considerations apply to cuts on other variables such as the net transverse momentum of the hadron pair,  $p_{T\text{pair}}$ . The comparison with E-706 data [12] is shown in FIG. 13 where



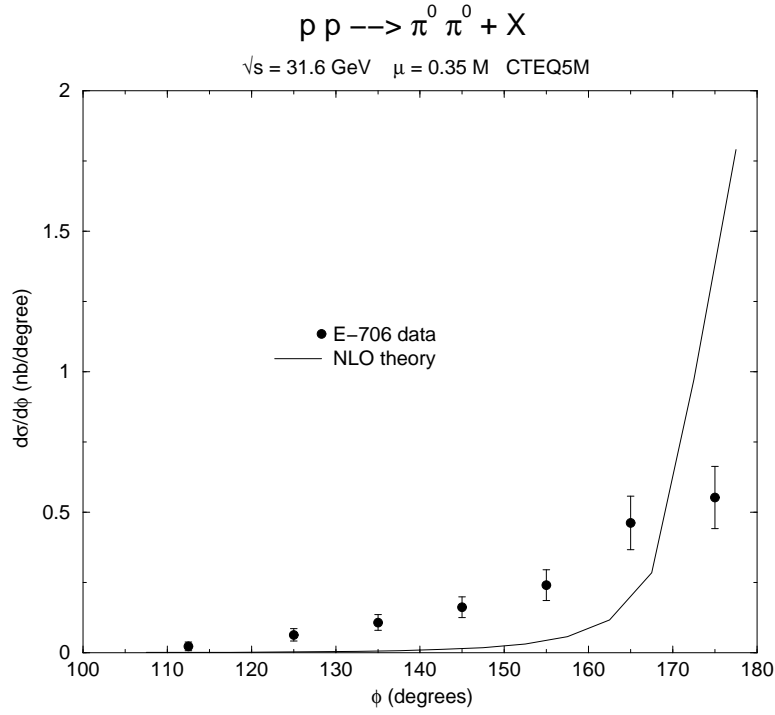


FIG. 11: Comparison of the NLO  $\Delta\phi$  distribution with data from E-706 [12].

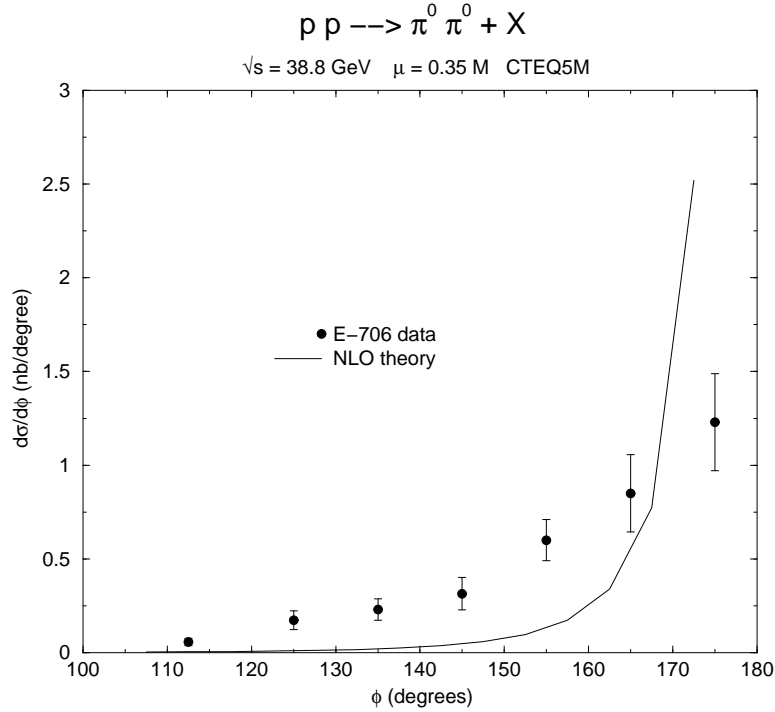


FIG. 12: Comparison of the NLO  $\Delta\phi$  distribution with data from E-706 [12].

one can see that the theoretical  $p_{Tpair}$  distribution is significantly narrower than is observed in the data. Comparisons to data which integrate over the full  $p_{Tpair}$  distribution will differ

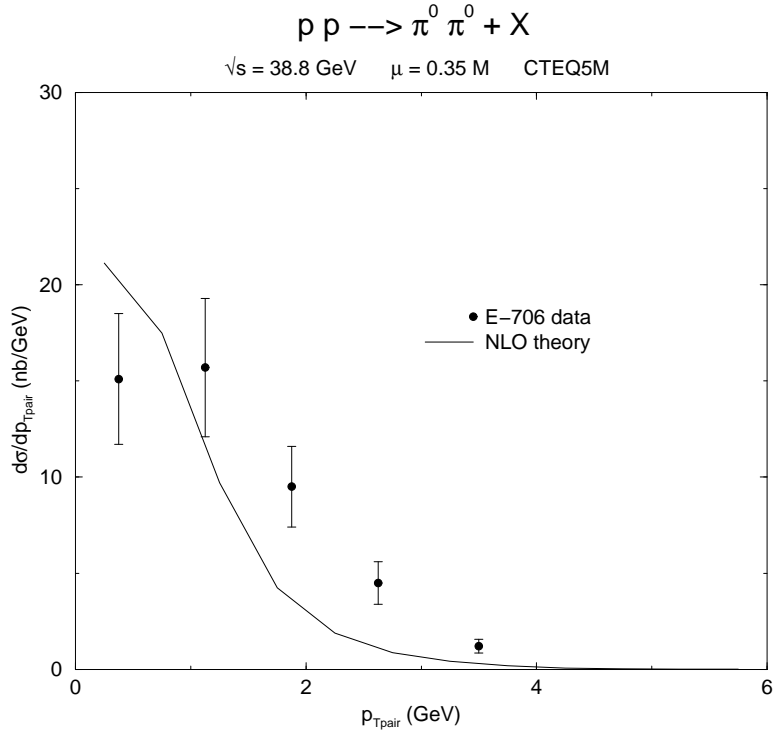


FIG. 13: Comparison of the NLO  $p_{Tpair}$  distribution with data from E-706 [12].

from comparisons to data sets which place cuts on this variable.

This situation should, in fact, come as no surprise. Both the  $\Delta\phi$  and  $p_{Tpair}$  distributions are examples which are delta functions at lowest order. Non-trivial contributions to these observables only start in next-to-leading order. In that sense, the curves shown here for these distributions are really leading-order only and they diverge at the endpoints corresponding to the third parton being soft and/or collinear ( $\Delta\phi = 180^\circ$  or  $p_{Tpair} = 0$ ). A more realistic treatment of these observables would require the application of soft gluon resummation techniques. Note, however, that there are compensating singularities at the endpoints of the distributions, so that a finite result is obtained after integrating over the distribution and the normalization of the integrated distribution is thus calculated to next-to-leading order.<sup>1</sup>

From the standpoint of comparing to NLO calculations, it would be better if the data sets were defined only by cuts on variables whose distributions are well described by the calculation. In this sense, the E-706 procedure is to be preferred since a large portion of both the  $\Delta\phi$  and  $p_{Tpair}$  distributions were integrated over.

<sup>1</sup> Due to the use of finite width bins, the divergent behavior at the endpoint of the  $p_{Tpair}$  distribution in FIG. 13 is not evident. The first bin remains finite as it contains the endpoint contribution, as well.

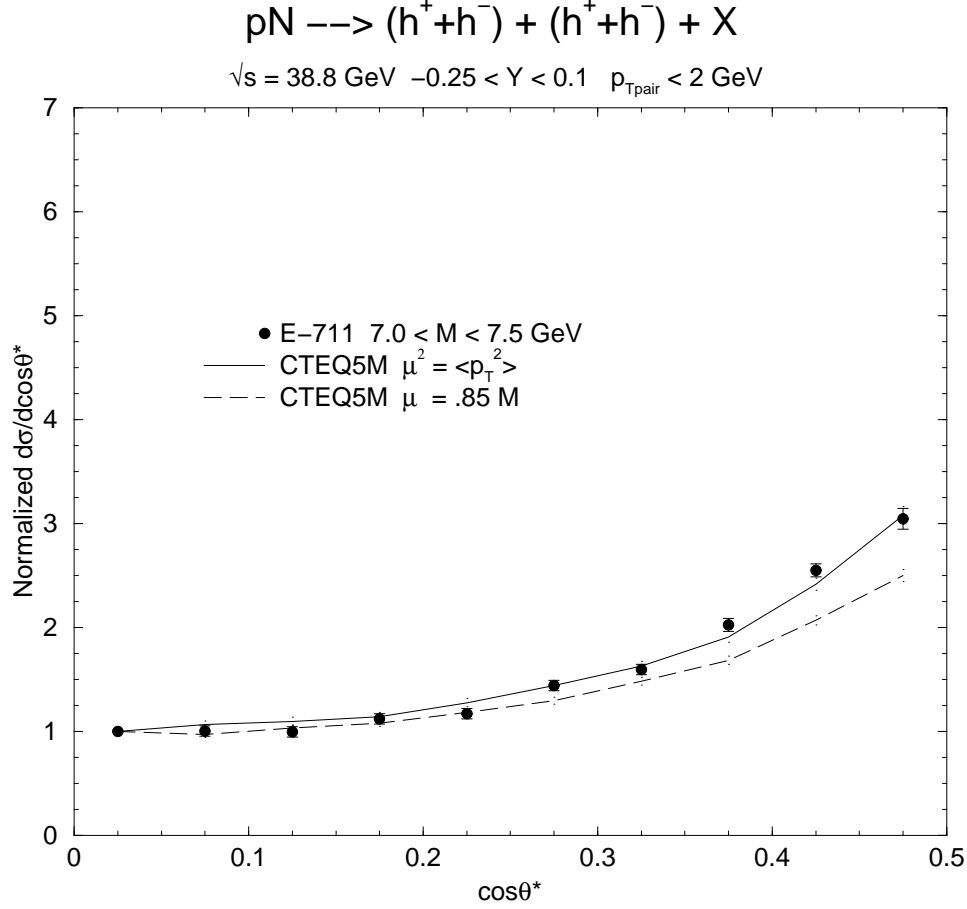


FIG. 14: Comparison between the CTEQ5M results and the E-711 angular distribution data for  $7 < M < 7.5 \text{ GeV}$  using two choices for the scale parameter.

The cuts utilized in the analysis of the E-706 data differ substantially from those which were used for the CCOR, NA-24, and E-711 data sets. Therefore, separate comparisons are required and the optimum choice of scale will differ between the two sets of experiments. It must be stressed that this is not an experimental problem, but rather the result of the fact that the NLO calculation does not properly describe the distributions in some of the variables used for making the cuts.

The E-711, E-706, and CCOR Collaborations each measured the angular distribution of the dihadron pair in the parton-parton center-of-momentum frame. None of the experiments observed any significant variation of this distribution with dihadron mass or with energy. The theoretical results for the normalized  $\cos\theta^*$  distribution are compared to the E-711 data [13, 17] in FIG. 14 for  $7 < M < 7.5 \text{ GeV}$  and in FIG. 15 for  $M > 7.5 \text{ GeV}$ . In each figure two curves are shown corresponding to the NLO results with scale choices of  $0.85M$  and

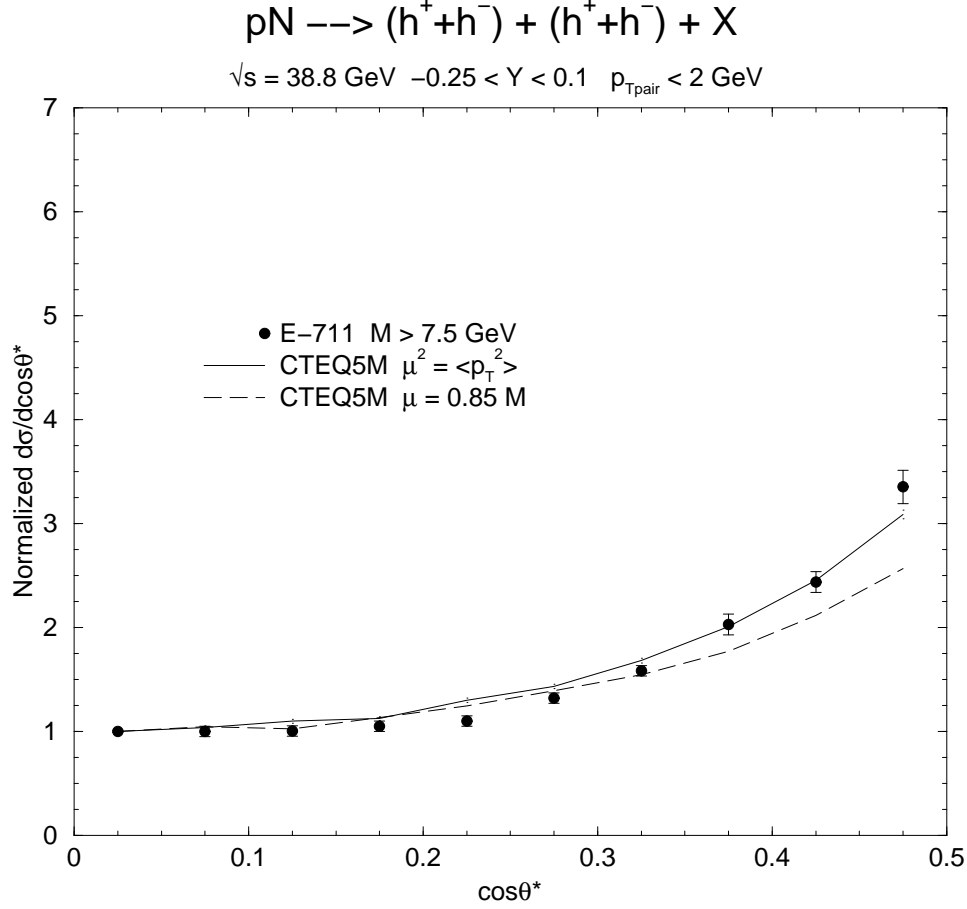


FIG. 15: Same as for FIG. 14 except for  $M > 7.5 \text{ GeV}$ .

$\sqrt{\langle p_T^2 \rangle}$ , where  $\langle p_T^2 \rangle$  is the average of the squared transverse momentum for the two observed hadrons in the event. Note that for the case of two-body kinematics at fixed  $M$ , the parton transverse momentum is  $\frac{M}{2} \sin \theta^*$  and the parton and hadron transverse momenta are nearly the same since the fragmentation variable  $z$  is near one. Thus, one can argue that for fixed  $M$  and  $\theta^*$  either  $M$  or  $\sqrt{\langle p_T^2 \rangle}$  is a valid choice for the scale. The choice of  $\sqrt{\langle p_T^2 \rangle}$  gives a steeper distribution which is in better agreement with the data than is the result obtained with the choice of  $0.85M$  for the scales. This steepening occurs because at fixed  $M$  as  $\cos \theta^* \rightarrow 1$ ,  $\sqrt{\langle p_T^2 \rangle}$  decreases. This decreasing scale causes an increase in the theoretical cross section. However, since the distribution is normalized to unity at  $\cos \theta^* = 0$ , the end result is a steeper angular distribution.

## IV. SUMMARY AND CONCLUSIONS

A next-to-leading-log Monte Carlo program has been constructed for symmetric dihadron production using the two cut-off phase space slicing formalism described in Refs. [4, 5]. This process serves as a probe of the underlying hard-scattering subprocesses which complements that provided by single particle production. For high mass pairs the relevant range of the fragmentation momentum fraction  $z$  is comparable to that for single particle production. The results presented here show that the NLO QCD formalism is capable of giving a good description of the data for the dihadron mass and angular distributions. There appears to be no anomalous behavior with respect to either the dihadron mass or the center-of-mass energy. This is in marked contrast to the cases for direct photon and single hadron production at fixed target energies. This process, therefore, provides encouraging evidence that the underlying hard scattering is correctly described by QCD and that the problems with the single photon and single hadron cross sections may be ascribed to a combination of effects due to an incomplete application of the theory and possible inconsistencies amongst the various data sets.

### Acknowledgments

The author wishes to thank Brian Harris for useful discussions.

- 
- [1] P.Aurenche et al., *Eur. Phys. J. C* **9**, 107 (1999).
  - [2] P. Aurenche et al., *Eur. Phys. J. C* **13**, 347 (2000).
  - [3] L. Apanasevich et al., *Phys. Rev. D* **59**, 074007 (1999).
  - [4] L. J. Bergmann, *Next-to-leading-log QCD calculation of symmetric dihadron production*, Ph.D. thesis, Florida State University, 1989.
  - [5] B.W. Harris and J.F. Owens, hep-ph/0102128, submitted to *Phys. Rev D*.
  - [6] R.K. Ellis and J.C. Sexton, *Nucl. Phys. B* **269**, 445 (1986).
  - [7] Z. Kunszt and D. E. Soper, *Phys. Rev. D* **46**, 192 (1992).
  - [8] B. A. Kniehl, G. Kramer, and B. Pötter, *Nucl. Phys. B* **582**, 514 (2000).
  - [9] L. Bourhis, M. Fontannaz, J.Ph. Guillet, and M. Werlen, *Eur. Phys. J. C* **19**, 89 (2001).

- [10] C. De Marzo et al., *Phys. Rev. D* **42**, 748 (1990).
- [11] A.L.S. Angelis et al., *Nucl. Phys. B* **209**, 284 (1982).
- [12] M. Begel, *Production of high mass pairs of direct photons and neutral mesons in a Tevatron fixed target experiment*, Ph.D. Thesis, Rochester University, 1999.
- [13] H.B. White et al., *Phys. Rev. D* **48**, 3996 (1993).
- [14] H.L. Lai et al., *Eur. Phys. J. C* **12**, 375 (2000)
- [15] A.D. Martin, R.G. Roberts, W.J. Stirling, and R.S. Thorne, *Eur. Phys. J. C* **4**, 463 (1998).
- [16] A.L.S. Angelis et al., *Phys. Lett. B* **79**, 505 (1978).
- [17] H.B. White, *A Study of Angular Dependence in Parton-Parton Scattering from Massive Hadron Pair Production*, Ph.D. Thesis, Florida State University, 1991.